GRAPHING THE WEIGHT 2 MODULAR FORM ATTACHED TO $X_0(11)$

Kevin T. Grosvenor

Harvard University
kgrosven@fas.harvard.edu

Freshman Seminar: Fermat's Last Theorem
Professor William Stein
was@math.harvard.edu
http://modular.fas.harvard.edu

Introduction

The deep connections that have been discovered between the concrete mathematical objects called *elliptic curves* and their highly esoteric cousins, the *modular forms*, have stimulated extraordinary and groundbreaking advances in such fields as Number Theory.

One such advance occurred in 1994 when Andrew Wiles, professor of mathematics at Princeton University in Princeton, NJ finally achieved what had until then eluded a veritable who's who of mathematics for nearly 300 years: he proved Fermat's Last Theorem. The collective genius of Euler, Germain, Legendre, Dirichlet, Lamé, Kummer, and countless others paled under the great complexity of the problem and while large improvements were manufactured, a general proof remained elusive.

Two discoveries were to provide giant leaps towards a general proof. These were the *Taniyama-Shimura-Weil Conjecture* and Gerhard Frey's *Epsilon Conjecture*. To give a full and detailed description of each of these would be beyond the scope of this paper. However, briefly, the first of these conjectures hypothesizes that, in fact, elliptic curves and modular forms are different representations of the same thing. The second conjecture states that any purported counterexample to Fermat's Last Theorem for a prime exponent greater than or equal to 5, produces an elliptic curve that is not modular.

Since the truly key factor in such advances as the proof of Fermat's Last Theorem can be traced down to this connection between elliptic curves and modular forms, this shall be the topic guiding this paper. It is a visual exploration of the weight 2 modular form attached to the elliptic curve called $X_0(11)$, which is given by the equation $y^2 + y = x^3 - x^2 - 10x - 20$.

1   Background Definitions

It is profitable to take a look at some of the background information that leads to the goal of this paper, which is to catch a glimpse of what the graph of the weight 2 modular form on $X_0(11)$ might look like.

Let us define terms before defining what we mean by modular form.

Definition 1.1: The *upper half plane* is the set of all complex numbers with imaginary part greater than zero. That is, the upper half plane, denoted **H**, is

$$\mathbf{H} = \left\{ z \in \mathbf{C} \mid \mathrm{Im}\, z > 0 \right\}$$

Definition 1.2: The *modular group* Γ is the set of all transformations in **C** of the following form (called linear fractional transformations):

$$\gamma(z) = \frac{az+b}{cz+d} \text{ where } a,b,c,d \text{ are integers and } ad - bc = 1$$

Definition 1.3: The quotient of Γ by the subgroup generated by $\{+1,-1\}$ is isomorphic to the group of 2×2 matrices with entries in **Z** and determinant 1, denoted by $\mathrm{SL}_2(\mathbf{Z})$:

$$\mathrm{SL}_2(\mathbf{Z}) = \left\{ \begin{bmatrix} a & b \\ c & d \end{bmatrix} \middle| a,b,c,d \in \mathbf{Z} \text{ and } ad - bc = 1 \right\}$$

So, for simplicity, we can represent $\gamma \in \Gamma$ by a matrix in $\mathrm{SL}_2(\mathbf{Z})$ and define:

$$\begin{bmatrix} a & b \\ c & d \end{bmatrix} \cdot z = \frac{az+b}{cz+d}$$

Definition 1.4: The sequence of numbers, denoted a_n, of an elliptic curve E with conductor N, are determined by the number of solutions there are for E in $\mathbf{Z}/p\mathbf{Z}$, denoted by N_p for prime integers p. They are governed by these rules:

(1) $a_p = p + 1 - N_p$ for prime integers p that do not divide N

(2) $a_{p^r} = a_{p^{r-1}} \cdot a_p - p \cdot a_{p^{r-2}}$ for prime integers p that do not divide N

(3) $a_{nm} = a_n \cdot a_m$ if $\gcd(n,m) = 1$

(4) $a_{s^n} = (a_s)^n = \pm 1, \quad \forall n \in \mathbf{Z}^+$ for s a prime divisor of N and $a_N = 1$

Since the conductor of $X_0(11)$ is 11, which is prime, we do not need to worry about primes p that do divide N.

2   The Modular Form on Elliptic Curves

We can now go ahead and describe the modular form attached to an elliptic curve.

Definition 2.1: The modular form associated to an elliptic curve with discriminant Δ, going from the upper half plane to the complex plane, denoted by $f_E : \mathbf{H} \to \mathbf{C}$, is defined by the following:

$$f_E(z) = \sum_{\substack{n=1 \\ \gcd(n,\Delta)=1}}^{\infty} a_n e^{2\pi i z n} \text{ with } a_n \text{ as defined in Definition 1.4}$$

For ease, we shall henceforth drop the E in the denotation of the modular function and simply write f.

Definition 2.2: With particular pertinence to the elliptic curve E on which f is defined, given N, the conductor of E, we define $\Gamma_0 \subset \Gamma$ where, in matrix form:

$$\Gamma_0(N) = \left\{ \begin{bmatrix} a & b \\ c & d \end{bmatrix} \in \mathrm{SL}_2(\mathbf{Z}) \ \middle| \ \text{N divides } c \right\}$$

Proposition: It is a fact that $f(z)\mathrm{d}z$ is invariant under the action of $\Gamma_0(N)$ and as a result the following holds for $\gamma \in \Gamma_0(N)$:

$$f \circ \gamma(z) = f\left(\frac{az+b}{cz+d}\right) = (cz+d)^2 f(z)$$

Proof: We have $f(z)\mathrm{d}z = f\left(\frac{az+b}{cz+d}\right) \cdot \mathrm{d}\left(\frac{az+b}{cz+d}\right) = f\left(\frac{az+b}{cz+d}\right) \cdot \frac{(cz+d)a-(az+b)c}{(cz+d)^2}\mathrm{d}z$ and thus, $f(z) = f\left(\frac{az+b}{cz+d}\right) \cdot \frac{(ca-ac)z+ad-bc}{(cz+d)^2} = f\left(\frac{az+b}{cz+d}\right) \cdot \frac{1}{(cz+d)^2}$. ∎

3   The Modular Domain and Fundamental Domain

We now begin to visualize the domain of the modular form. It seems to be a daunting task to try to visualize how the modular function f transforms the entire upper half plane. However, the concept of the Fundamental Domain will prove to be of significant help.

We will not go into the details of the theory behind how we might determine the Modular Domain, denoted D, and hence the fundamental domain, denoted $\overline{\text{D}}$ (see Goldman chapter 12.9, 13.1 and 13.2).

Definition 3.1: Suffice it to say that $z \in \text{D}$ provided that:

$$(1) \quad -\tfrac{1}{2} \le \operatorname{Re} z \le 0 \text{ and } |z| \ge 1; \text{ or}$$

$$(2) \quad 0 < \operatorname{Re} z < \tfrac{1}{2} \text{ and } |z| > 1$$
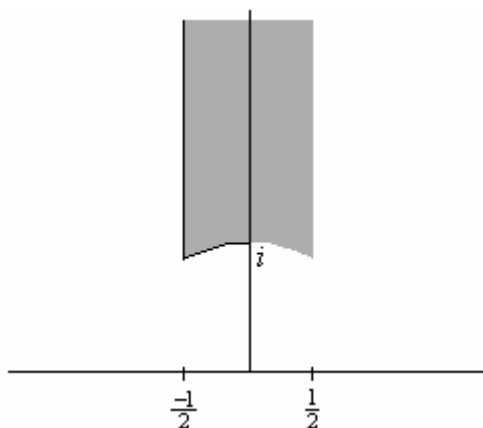
Thus, D looks like the following figure 1:

Figure 1: The Modular Domain

Definition 3.2: The Fundamental Domain for Γ is the closure of D, denoted by $\overline{\text{D}}$, and is simply D with the boundaries included.

In order to make further discussion on the Fundamental Domain, we must introduce the two linear fractional transformations that generate Γ.

Proposition: The following two matrices S and T generate Γ:

$$S = \begin{bmatrix} 0 & -1 \\ 1 & 0 \end{bmatrix} \text{ and therefore, } Sz = \tfrac{-1}{z} \text{ ; and } T = \begin{bmatrix} 1 & 1 \\ 0 & 1 \end{bmatrix} \text{ and so, } Tz = z + 1$$

Now, a very important claim can be made, which will justify precisely why we name the fundamental domain thus.

Theorem: For all z in **H**, there exists a γ in Γ such that $\gamma z \in \overline{D}$.

Proof: Only the procedure for actually finding γ shall be shown here. In truth, one would need to show that this procedure actually terminates in finitely many steps (see Goldman chapter 13.5).

The procedure for finding the particular γ in Γ that will map z into something in the fundamental domain can be found in flow chart form in Goldman's book "The Queen of Mathematics" and is reproduced here. First, we must label the complex number as z_0 as this process may need to be iterated several times before producing a z_i in the fundamental domain. In figure 2, S and T are the generators of Γ given previously.
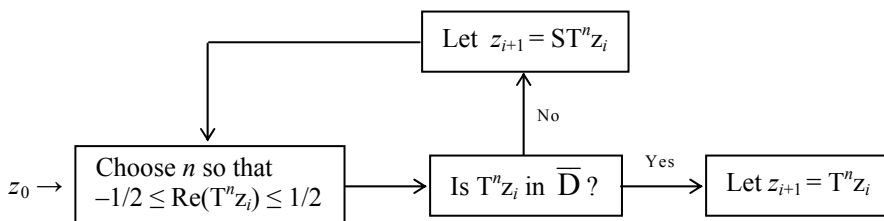

Figure 2: Using S and T to map z into $\overline{D}$

Clearly, after going through this flow chart however many times necessary, we will have:

$$z_{i+1} = S^{m_1} T^{n_1} S^{m_2} T^{n_2} \cdots z_0 \text{ and therefore, } \gamma = S^{m_1} T^{n_1} S^{m_2} T^{n_2} \cdots$$

Therefore, in the next section, we shall examine the image of $\overline{D}$ under certain combinations of S and T.

5

4   S-T Transformations of the Fundamental Domain

Given the definitions of S and T, it is clear to see that what S does to z is it inverts it with respect to the unit circle and then reflects this inversion over the y-axis, and what T does is it translates z one unit to the right. Hence the following is a diagram which bounds certain areas corresponding to where a particular combination of S and T maps the fundamental domain. This diagram and its derivation and explanation can be found in Goldman chapter 13.5.
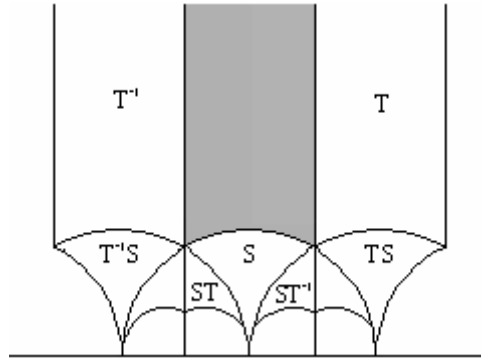

Figure 3: Transformations of $\overline{\mathrm{D}}$ under S and T

Therefore, it appears that if we were able to relate the values of f on $\overline{\mathrm{D}}$ to its values on the area marked S in figure 3, then, we can find the values of f on the fundamental domain by computing f in S.

Unfortunately, the only similar relationship available to us is that described in the proposition in Section 2 on page 3. This relationship only holds for Γ_0 and since the conductor of $X_0(11)$ is 11 and 11 does not divide 1, $S \notin \Gamma_0(11)$.

Therefore, instead, we must examine the fundamental domain not of Γ, but of $\Gamma_0(11)$.

5   Generators and Fundamental Domain of $\Gamma_0(11)$

Since we do not have the wonderful relationship between $f(\gamma z)$ and $f(z)$, which we showed in section 2, unless γ is in $\Gamma_0(N)$, we must work instead with the generators and fundamental domain of $\Gamma_0(N)$.

We shall use programs to give us the answers. As stated earlier, $X_0(11)$ has conductor $N = 11$.

In William Stein's website is a PARI/MAGMA calculator, which we use to find the generators of $\Gamma_0(11)$. The URL for the calculator page is given here: http://modular.fas.harvard.edu/calc.

Thus, we have the generators of $\Gamma_0(11)$:

$$T = \begin{bmatrix} 1 & 1 \\ 0 & 1 \end{bmatrix}, \ U = \begin{bmatrix} 3 & -2 \\ 11 & -7 \end{bmatrix}, \text{ and } V = \begin{bmatrix} 4 & -3 \\ 11 & -8 \end{bmatrix}$$

In order to visualize the image of the fundamental domain under these transformations, we use Helena Verrill's website, which draws fundamental domains for several subgroups of Γ. The URL is http://hverrill.net/fundomain/index2.html.

Figure 4 shows a snapshot of the fundamental domain drawer as it has drawn the fundamental domain for $\Gamma_0(11)$.
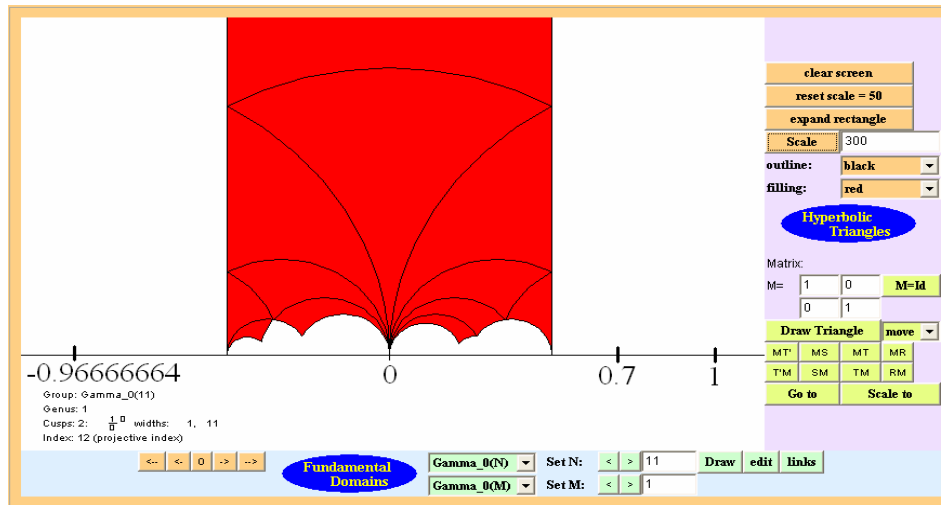

Figure 4: The Fundamental Domain of $\Gamma_0(11)$

Notice that the fundamental domain for $\Gamma_0(11)$ is divided into 12 hyperbolic triangles. This arises from a result, which we shall not discuss in great detail here, but which we shall mention briefly now.

There is a theorem that states that if H is a subset of G, then G can be written as the disjoint union of the left cosets of H by elements of a subset R of G. That is, if $H, R \subseteq G$ then $G = \bigcup_{r \in R} rH$. So, we have that $\Gamma = \bigcup_{\gamma \in \Gamma'} \gamma \Gamma_0(N)$.

Then, another theorem says that if N is prime, then $\Gamma' \subseteq \Gamma$ will contain $N+1$ elements. Thus, the fundamental domain of $\Gamma_0(11)$ will contain twelve images of the fundamental domain of Γ each image being under one element of Γ. Recall, however, that S and T, as we defined them earlier, generate Γ, and so we should be able to write each of these transformations in terms of S and T. The following diagram shows exactly what the twelve transformations are.
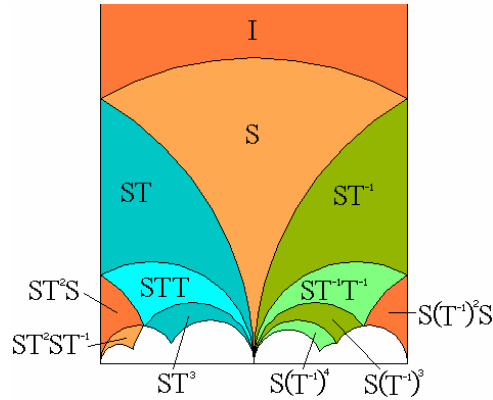

Figure 5: The transformations comprising the fundamental domain of $\Gamma_0(N)$

Therefore, we can map all of H into the fundamental domain of Γ by first applying a transformation in $\Gamma_0(11)$ and then applying one of these twelve transformations in Γ. Thus, logically, using $\Gamma_0(11)$, we can map all of H into the image of the fundamental domain of Γ under one of these twelve transformations, which includes the domain itself by the identity map, I. Thus, figure 5 is the fundamental domain of $\Gamma_0(11)$.

We now look at how U and V transform this fundamental domain. The colors in figure 6 correspond with those in figure 5.
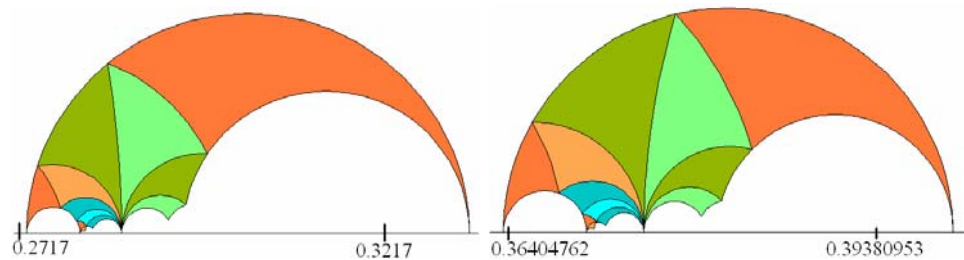

Figure 6: Transformation of the fundamental domain of $\Gamma_0(11)$ under U and V

8

Since T is in $\Gamma_0(11)$, a large portion of the upper half plane is already covered by the fundamental domain and its image under iterations of T and T^{-1}. In fact, the only area left is that underneath the fundamental domain. Thus, we must search for the right combinations of T, U, and V that map the fundamental domain in to the space directly underneath it.

This is not the simplest of tasks. The author was able to cover only two main portions of this area and chose instead to extend the fundamental domain and make it symmetric along the imaginary axis for simplicity. The following diagram shows the two portions under the fundamental domain for $\Gamma_0(11)$, which the author managed to fill in. Successive magnifications are on the right and the bottom right image indicates the positions of the images of the fundamental domain under U and V as shown in figure 6 on the previous page. The area under the fundamental domain and to the right is covered using the transformations U, V, UT, and VT. The area to the left is covered using the transformations $(UT)^{-1}$ and $(VT)^{-1}$.
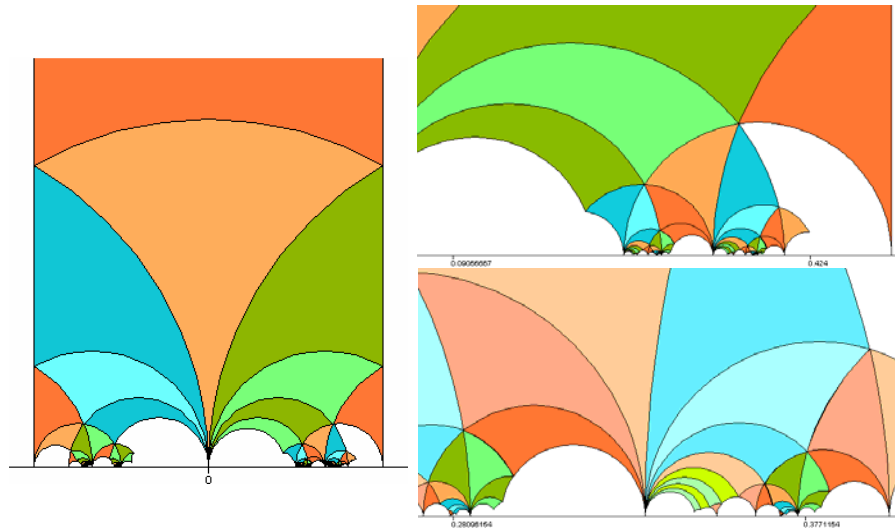

Figure 7: Two areas under the fundamental domain covered by some $\gamma \in \Gamma_0(11)$ with successive magnifications on the right

6   Atkin-Lehner Involution

It is a fact that as z approaches the real axis, that is as the imaginary part of z approaches 0, f converges more and more slowly. As it turns out, the graph of f seems to increase dramatically in complexity and curiosity as z approaches the real axis. This arises from the fact that smaller and smaller areas below the fundamental domain can be covered with various combinations of T, U, and V, the generators of $\Gamma_0(11)$, and there is a relationship between the value of f in these smaller and smaller areas to its value over the entire fundamental domain. Thus, f is fractal-like as z approaches the real axis.

Fortunately, there is a technique available for calculating f very close to the origin, which may be of significant help, called Atkin-Lehner Involution.

We will not detail how the Atkin-Lehner Involution method can be deduced, but will show how it works. Instead of using γ in Γ, we use the matrix:

$$g = \begin{bmatrix} 0 & -1 \\ N & 0 \end{bmatrix}$$ where N is the conductor. If $\operatorname{Im} z \to 0$, then $\operatorname{Im} gz = \operatorname{Im} \frac{-1}{Nz} \to \infty$.

Atkin-Lehner involution gives $f(z) = \pm (Nz)^{-2} \cdot N \cdot f\left(\frac{-1}{Nz}\right)$. Thus, we can find $f(z)$ for z close to the real axis indirectly by finding f on a point far from the real axis where f will converge well.

In the following section we discuss PARI, which is the program we use to calculate f at certain points. Using a function in PARI, we can determine the sign in the above equation.

7 PARI gp

We must now introduce the program PARI, which is the program we shall use to calculate the value of f at certain points. The following are the five built-in PARI functions that we will need to use: `ellinit`, `ellan`, `ellrootno`, `sum`, and `exp`.

Elliptic curves can be defined by five variables a_1, a_2, a_3, a_4, a_5 in PARI corresponding to the equation $y^2 + a_1 xy + a_3 y = x^3 + a_2 x^2 + a_4 x + a_5$.

`ellinit([a₁,a₂,a₃,a₄,a₅])` enters the corresponding elliptic curve into PARI, which we will ordinarily store into the variable e. Thus, according to the equation of $X_0(11)$, we enter it as `[0,-1,1,-10,-20]`.

`ellan(e,n)` lists the sequence described in Definition 1.4 for elliptic curve e from a_1 to a_n.

`sum(n=1,max n, function)` will compute $\sum_{n=1}^{\max n} f(n)$ and `exp(m)` will raise Euler's number e (not elliptic curve e) to the power of m.

Finally, to determine the sign for the Atkin-Lehner involution, discussed in the previous section, we enter `-ellrootno(e)` with the negative sign. If this equals 1, then the involution sign is plus; if it is -1, then the sign is minus.

Ordinarily, we use the functions `ellglobalred` and `ellchangecurve` to transform the elliptic curve into minimal form. However, $X_0(11)$ is already in minimal form and thus we do not need to worry about this.

The following image is a snapshot of the PARI gp screen with the commands in place. We enter $X_0(11)$ given by [0,-1,1,-10,-20]. We also show a value of f calculated the normal way, which is negative of that found using involution. But, notice how many more terms are needed for f to converge well as opposed to f_atkin, which is what we have denoted Atkin-Lehner Involution.


```
parisize = 4000000, primelimit = 500000
(01:20) gp > e=ellinit([0,-1,1,-10,-20]);
(01:20) gp > N=11;
(01:20) gp > v=ellan(e,200000);
(01:21) gp > m(z)=exp(2*Pi*I*z)
(01:21) gp > g(z)=exp(-2*Pi*I/(N*z))
(01:21) gp > f(z,terms)=k=m(z); sum(n=1,terms,v[n]*k^n)
(01:21) gp > f_atkin(z,terms)=k=g(z); ((N*z)^-2)*N*sum(n=1,terms,v[n]*k^n)
(01:22) gp > -ellrootno(e)
%4 = -1
(01:22) gp > z=-.19+.06244998*I; f(z,1000)
%5 = 1.4881577332883023734778851164 + 0.2316813350984504873182499167*I
(01:22) gp > z=-.19+.06244998*I; -f_atkin(z,50)
%6 = 1.4881577332883023733954855674 + 0.2316813350984504873183312718*I
(01:22) gp >
```

Figure 8: Snapshot of PARI gp screen

8 Bounding the Errors

Since f is defined by an infinite sum (and not a simple one such as an arithmetic or geometric series) it is impossible for PARI to calculate it exactly. Thus, the values that we will get from PARI will be approximations. However, for the most part, these approximations will be extremely accurate for we will try to calculate f at points where convergence is exceptional.

Nevertheless, we must bound the error that is created by truncating the sum at the number of terms to which we take the sum in PARI. To do this, we use the fact that $|a_n| \leq n$ for all natural numbers n.

Proposition: If we truncate $f(z)$ to a sum from $n = 1$ to $n = k$, and we are given that $|z| < 1$, then the error term, denoted by δ, satisfies the following inequality:

$$\delta \leq p^{k+1} \left(\tfrac{1}{1-p} \right)^2 \left(k(1-p) + 1 \right) \text{ where } p = |q| \text{ and } q = e^{2\pi i z}.$$

Proof: $\sum_{n=1}^{\infty} a_n q^n = \sum_{n=1}^{k} a_n q^n + \sum_{n=k+1}^{\infty} a_n q^n$. The last term is the error. Thus,

$\delta = \left| \sum_{n=k+1}^{\infty} a_n q^n \right| \leq \sum_{n=k+1}^{\infty} |a_n| \cdot |q|^n \leq \sum_{n=k+1}^{\infty} n \cdot |q|^n$. Letting $p = |q|$, we have that

$$\begin{aligned}
\sum_{n=k+1}^{\infty} n \cdot |q|^n &= (k+1)p^{k+1} + (k+2)p^{k+2} + (k+3)p^{k+3} + \ldots \\
&= kp^{k+1}\left(1 + p + p^2 + \ldots\right) + p^{k+1}\left(1 + p + p^2 + \ldots\right) + p^{k+2}\left(1 + p + p^2 + \ldots\right) \\
&= kp^{k+1}\left(1 + p + p^2 + \ldots\right) + p^{k+1}\left(1 + p + p^2 + \ldots\right)\left(1 + p + p^2 + \ldots\right) \\
&= kp^{k+1}\left(\tfrac{1}{1-p}\right) + p^{k+1}\left(\tfrac{1}{1-p}\right)^2 \\
&= p^{k+1}\left(\tfrac{1}{1-p}\right)^2 \left(k(1-p) + 1\right) \quad \blacksquare
\end{aligned}$$

We note that since we must have $|z| < 1$, this bound is not very useful for calculating f the regular way since as we can see, the smaller p is (and therefore, the closer z is to the real axis), the larger k must be in order to keep δ small.

Clearly, however, the important thing is not simply to keep the error small, but to keep it small relative to the actual value calculated (the truncated sum). We do not need to delve into the theory of this. Instead, in calculating some of the values of f, the author checked that the upper bound for the error, which is likely to be considerably larger than the actual error, was much smaller in comparison to the calculated values.

9   The Image of some Semicircles under f

Using the method of Atkin-Lehner Involution, I calculated the values of $f(z)$ for z lying on some semicircles in $\mathbf{C}$. We do this since, if we use involution, then,

$$|q| = \left| e^{\frac{-2\pi i}{Nz}} \right| = \left| e^{\frac{-2\pi i}{N(x+iy)}} \right| = \left| e^{\frac{2\pi iy}{N\left(x^2+y^2\right)}} \right| = \left| e^{\frac{2\pi iy}{N|z|^2}} \right|$$

Thus, $|q|$ depends on $|z|$, among other factors.

First we show the graph of the semicircles, and then their image under f. The top right is the image of the semicircle of radius 1, then the middle left is radius 0.9, middle right is radius 0.8, bottom left is radius 0.7, and bottom right is radius 0.6.
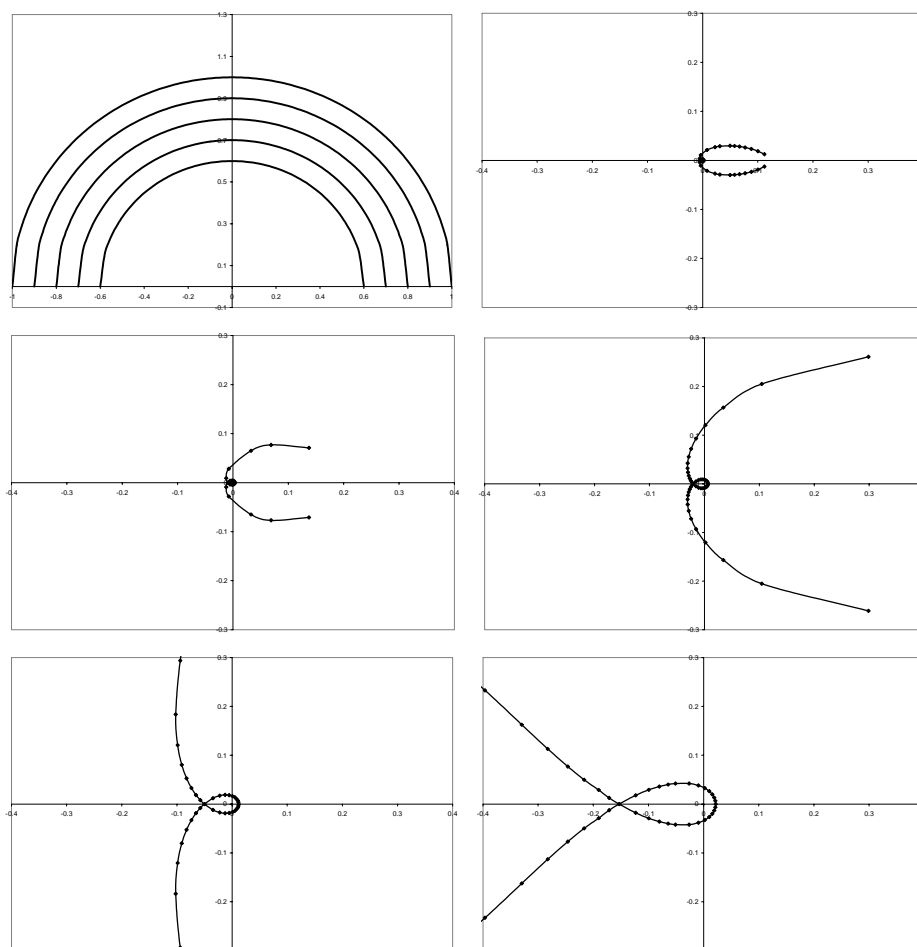

Figure 9: Graphs of the semicircles and their images under f

13

10 Domain Coloring and Graphing the Argument

Since we would have to make a four-dimensional graph in order to fully show how f transforms the upper-half plane, we instead have to use other techniques such as the one shown in the previous section, which is showing what happens to certain curves or lines. Another technique is to ignore one of the dimension altogether.

For this latter approach, it would be almost meaningless to totally ignore either the real coordinate or the imaginary coordinate. Instead, we transform the complex values of f into polar coordinates, that is we have the magnitude and the argument of the calculated values of f. Then, it might be fruitful to focus solely on the argument or the magnitude. These can be graphed separately thus making two 3D graphs. Or, we can use a technique that is often called Domain Coloring. In our case, we make a correspondence between an argument $\arg(z) \in [0, 2\pi)$ radians or $\arg(z) \in [0, 360)$ degrees and a color. Then, we color the point at which f is evaluated by the color corresponding to the argument of the value of f at that point.

To do this, the author calculated f for the points with real part from -0.50 to 0.00 by intervals of 0.02 and imaginary part from 0.01 to 0.10 by intervals of 0.01.

There is probably a better way to graph this, perhaps with a program such as Mathematica, Maple, or GNUplot. However, the author is unversed in these programs and thus instead used Microsoft Paint! While keeping the color parameter *saturation* constant at 240 and *luminosity* at 120, the parameter *hue* was varied from 0 to 239. Thus, we have the color corresponding to argument by the following equation (the $\approx$ symbol is used because the right hand side must be rounded to the nearest integer):

$$hue(z) \approx \frac{\arg(f(z))}{2\pi} \cdot 240 = \frac{120}{\pi} \arg(f(z)) \text{ in radians or}$$

$$hue(z) \approx \frac{\arg(f(z))}{360} \cdot 240 = \frac{2}{3} \arg(f(z)) \text{ in degrees.}$$

Thus, the following image is the result of this technique done to the values of f at the particular points previously mentioned. Note that there are white spaces near the bottom. These correspond to the space that the author managed to cover using the transformations $(UT)^{-1}$ and $(VT)^{-1}$. We chose not to calculate the points there because we would later fill it in using the relationship:

$$f \circ \gamma(z) = (cz + d)^2 f(z) \text{ when } \gamma \in \Gamma_0$$

However, unfortunately, due to the tediousness of the process of making this graph alone, the author is yet unable to produce a detailed picture for this space. The reader might notice that we chose to fill in some of the other spaces under the fundamental domain that we were unable to cover using a combination of T, U, and V. This was done simply out of curiosity and because we were not going to find f at those points any other way anyway.
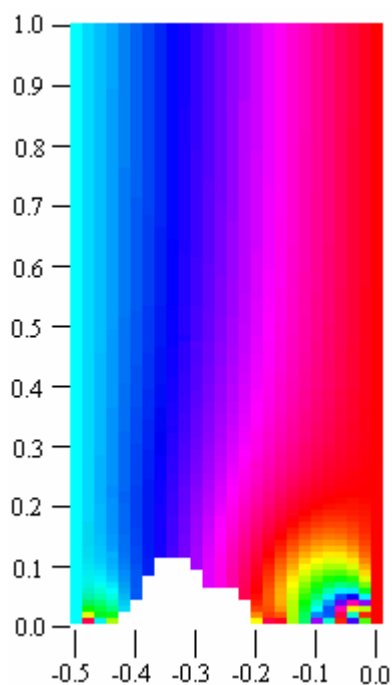
Figure 10: An image by Domain Coloring of the Argument of the values of f

As a brief explanation of the picture above, roughly speaking, $0°$ begins at red, then, rotating anti-clockwise, the color turns orange, yellow, and yellow-green at $90°$. Then, the color turns green and turns into light blue at $180°$. This color turns into the full blue that dominates the left side of the image above and then the transition from blue to purple occurs at $270°$. Finally, this color gradually transforms back into red.

Fortunately, if we use T^n as our transformation, we have $(cz+d)^2 = n^2$ and therefore, $f \circ T^n(z) = n^2 f(z)$, which keeps the argument invariant. Therefore, if we complete the image above up to 0.5, then f over the entire upper half plane would simply be the same image translated horizontally left and right repeatedly by 1.

It is interesting to note that, despite the low resolution, it still appears that the graph is continuous. This is a good sign because f is holomorphic, which means that it is differentiable at all points in the upper half plane and therefore, its graph must be continuous. Also, at the points near the real axis, the graph increases in complexity even at this low resolution. This is a good indicator of the fractal-like nature of the graph near the real axis.

15

11   Closing Statement

As is ever clearer, there is much left to do in this topic. A complete picture over the whole fundamental domain for $X_0(11)$ is on the way, but in order for sufficiently detailed graphs to be made we must automate the process of evaluating f. However, as it is, it is likely that a beautiful and significantly detailed picture of f in the small areas under the fundamental domain that I have covered with some combinations of T, U, and V can be made. However, I, for one, will be looking to other programs better suited to these rigorous tasks than is Microsoft Paint.

It would also be very interesting to examine how the graphs of these modular forms vary as the elliptic curve to which they are attached are changed.

12   Acknowledgements

REFERENCES

Goldman, Jay R. The Queen of Mathematics. Wellesley, MA: A.K. Peters, 1998

Stein, William. PARI & MAGMA Calculator. 7 Sept. 2004. Harvard University.
    15 Sept. 2004. <http://modular.fas.harvard.edu/calc>

Verrill, Helena. Fundamental Domain Drawer. Accessed: 17 Dec. 2004.
    <http://hverrill.net/fundomain/index2.html>